Published by IOP Publishing for Sissa Medialab

Received: *November 4, 2016*
Revised: *December 28, 2016*
Accepted: *February 23, 2017*
Published: *March 21, 2017*

TECHNICAL REPORT

ADRC control of a 6-DOF parallel manipulator for telescope secondary mirror

Y. Ye,[1] **Z. Yue and B. Gu**

National Astronomical Observatories/Nanjing Institute of Astronomical Optics & Technology, Chinese Academy of Sciences, 188 Bancang Street, Nanjing, 210042 China
Key Laboratory of Astronomical Optics & Technology, Nanjing Institute of Astronomical Optics & Technology, Chinese Academy of Sciences, 188 Bancang Street, Nanjing, 210042 China
University of Chinese Academy of Sciences, No. 19A Yuquanlu, Beijing, 100049 China

E-mail: yye@niaot.ac.cn

Abstract: In view of the special requirements of the secondary mirror control system on large aperture telescopes, an improved 6-DOF parallel manipulator is designed and used to replace the traditional hexapod used in telescope secondary mirror position dynamic compensation. A highly robust active disturbance rejection controller (ADRC) is designed, which consists of a nonlinear tracking differentiator (NTD), an extended state observer (ESO), a nonlinear state error feedback law (NLSEF), and disturbance compensation. The ESO can track the all-order state variables, as well as estimate and compensate for unmodeled dynamics and total external disturbance of the system. The results of simulation indicate that the ADRC can improve tracking precision and control performance when it is compared with the proportion integration differentiation (PID) controller. The test results show that the absolute accuracy of the three dimensional parallel motions is about $\pm 4\,\mu$m, and the two dimensional tilts' is about $10\,\mu$rad. The control precision meets the system design for a telescope secondary mirror.

Keywords: Control systems; Instrument optimisation; Simulation methods and programs

[1]Corresponding author.

doi:10.1088/1748-0221/12/03/T03006

2017 JINST 12 T03006

Contents

2017 JINST 12 T03006

1 Introduction

In a large aperture optical/infrared telescope, the relative position of the primary and secondary mirrors has a strong influence on the optical imaging quality of the telescope. The main factors that affect the relative position include gravity deformation, structure thermal deformation, and temperature gradient. It is difficult to change the primary mirror's position due to its heavy mass and large volume, so active optical technology has been used to change the mirror's shape. The relative position of the primary and secondary mirrors predominantly depends on adjusting the secondary mirror's pose. The secondary mirror's positioning capability allows the correction of defocus and coma optical aberrations, which are usually caused by incorrect relative positions of the optics [1].

Extremely large aperture telescopes, such as VLT [2], VST [3], GTC [4] and LGBT [5] adopt the conventional Stewart parallel platform for the secondary mirror structure. The Stewart platform is a 6-DOF parallel mechanism, which consists of a moving platform, a fixed base, and six limbs. The Stewart platform has several advantages: simple structure, high stiffness, non-cumulative error, etc. However, when it is used as the support system for the secondary mirror, the size and weight of the Stewart platform are restricted. The maximum allowed radial dimension of the platform must be less than the diameter of the secondary mirror. The axial dimension and the weight of the platform are restricted by the stiffness of the telescope wing and the serrurier truss. In order to solve these contradictions, a new hexapod mechanical structure was designed.

The 6-DOF parallel manipulator is a Multiple Input Multiple Output (MIMO) nonlinear system. Each joint has serious coupling inertia and interference between components, so controlled research on 6-DOF parallel manipulator is facing great challenges. There are many control methods being proposed to resolve this problem. These methods include adaptive control [6], slide control [7],

compound control [8], and Active Disturbance Rejection Control (ADRC) [9]. ADRC as a potential solution has been explored in many fields of control engineering, such as motor systems, flight control, robotic control, thermal processes, and in electromechanical systems and power electronics devices. ADRC is primarily comprised of four parts: a nonlinear tracking differentiator (NTD), an extended state observer (ESO), a nonlinear state error feedback law (NLSEF) and disturbance compensation [10]. It is a control algorithm that satisfies the requirements of the hexapod for the telescope's secondary control system.

2 Structure

The traditional Stewart platform is the SPS platform: the length of its six limbs can be changed [11]. In contrast, the new design is the PSS platform and its six rigid limbs slide on a guide. Figure 1 shows the two mechanical structures. In regard to the modelling and simulation of the new scheme, the reader can refer to the authors' another article (Modeling and Simulation of a 6-DOF Parallel Platform for Telescope Secondary Mirror) [12]. The advantages of the PSS hexapod in comparison to the SPS hexapod are listed as follows:

- Small structure and big absorbing load, with similar axial and radial load rating capacity.
- Shorter axial structure size and reduced length of the tube.
- Easy to arrange and fix all the driving components in the same radial plane and less heat produced by the driving components.
- Structure stiffness and vibration characteristics are more stable.

The secondary mirror of telescopes, for its special location in the equipment, has strict requirements on its bearings, the hexapod, on radial dimension and temperature control. The stress state of moving platform and fixed platform closely related to the elevating angle of the telescope, normally with

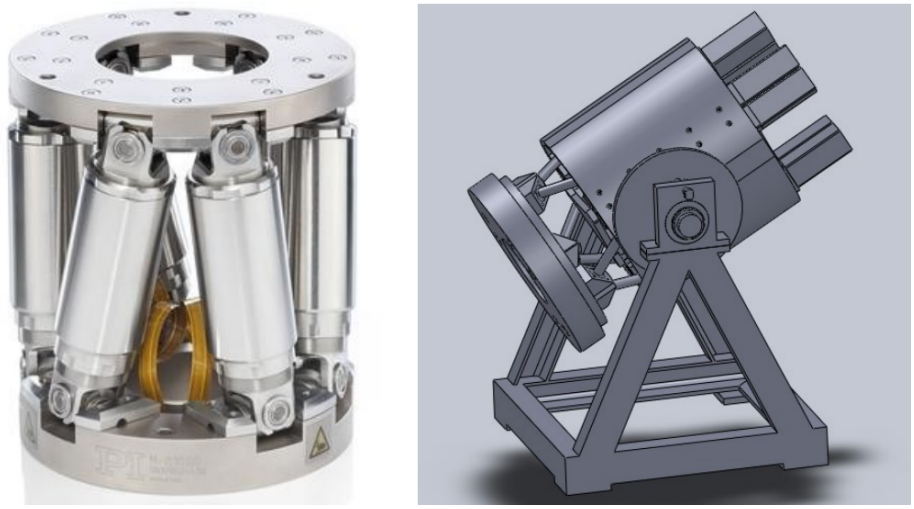

Figure 1. SPS hexapod (left) and PSS hexapod (right).

2017 JINST 12 T03006

great driving force. When great driving force required, the restrictions of radial dimensions caused difficulty in traditional structural arrangement. However, the new proposal could fully utilize the back space arrangement for actuator with greater driving force. When temperature control required, the temperature control structure wiggled, as the motor of heat dissipation, along with the waver of the rod in the traditional method, increasing the radial dimension of the rod and the possibility of rod interference. The new method makes it easy for locating the temperature control structure because the motor, for heat dissipation, is fixed in the back of the equipment.

According to the characteristics of the secondary mirror of the telescope, a new type of hexapod prototype model has been designed. The secondary mirror hexapod unit technical requirements are listed in table 1. These values are for a load weighting 20 kg. The maximum allowed radial dimension is 300 mm.

Table 1. Hexapod unit technical requirements.

Hexapod Performance	Focus	Centering	Tilt
Range	±6 mm	±3 mm	±20 arcmin
Absolute Accuracy	±8 μm	±8 μm	10 μrad
Max Speed	0.25 mm/s	0.25 mm/s	2 mrad/s
Resolution	0.5 μm	0.5 μm	1 μrad

3 Kinematics

The hexapod, for bearing secondary mirror of telescopes, must control the relative positions and angles of the moving platform and fixed platform. There were two ways in calculating the correlation of the target position and angle of the moving platform with the actuator range of motion: normal solving process and inverse method. The solving process is to calculate the position and angle of the moving platform by the actuator range of motion, while the inverse method does it in the reverse way. We have solved the forward kinematic of the hexapod which is using the trajectory equation of the straight line, rotation transformation matrix, translational transformation matrix and spherical equation to establish with six legs change length of known value of 6 quadratic equations, and to calculate six dimensional positions and postures of the moving platform. But in the practical application, the inverse method is usually adopted.

If the target position of the moving platform is known, the displacements of the six legs can be calculated. The detailed derivation process is as follows: a global reference frame XYZ is set up in the center of the fixed platform and a local coordinate system $X'Y'Z'$ is set up in the center of the moving platform. The position of the moving platform is broken down to the local coordinate system origin space position $O'(x, y, z)$ in the global reference frame. The transformation matrix is

$$\begin{bmatrix} \cos\gamma\cos\beta & \sin\gamma\cos\alpha + \cos\gamma\sin\beta\sin\alpha & \sin\gamma\sin\alpha - \cos\gamma\sin\beta\cos\alpha \\ -\sin\gamma\cos\beta & \cos\gamma\cos\alpha - \sin\gamma\sin\beta\sin\alpha & \cos\gamma\sin\alpha + \sin\gamma\sin\beta\cos\alpha \\ \sin\beta & -\cos\beta\sin\alpha & \cos\beta\cos\alpha \end{bmatrix}$$

where α, β, γ are the precession angle, nutation angle, and self-rotation angle, respectively. In this system, we use one (denoted by A) spherical hinge in the moving platform as an example. The

central target position of A is (x'_A, y'_A, z'_A), and the corresponding central position of fixed platform is (x_{0A}, y_{0A}, z_A). The distance, R, from the central position of the spherical hinge between the moving platform and the fixed platform is unchanged.

$$\begin{cases} R^2 = (x_{0A} - x'_A)^2 + (y_{0A} - y'_A)^2 + (z_A - z'_A)^2 \\ x_{0A} = x_{01} \\ y_{0A} = y_{01} \end{cases}$$

$x_{0A} = x_{01}$ and $y_{0A} = y_{01}$ are known. x'_A, y'_A, z'_A can be solved from the transformation matrix and the initial position vector arithmetic. Only z_A is unknown.

The central theoretical position of the spherical hinge (A) in the fixed platform is:

$$z_A = \sqrt{R^2 - (x_{0A} - x'_A)^2 - (y_{0A} - y'_A)^2} + z'_A \,.$$

In the same way, the other central theoretical positions of the spherical hinges in the fixed platform can be determined.

4 Active Disturbance Rejection Controller (ADRC)

In this system, an ADRC with model compensation is designed, which can improve the ESO estimation of the unknown parts of the controlled plant model. Figure 2 shows the ADRC structure with a model compensation system.

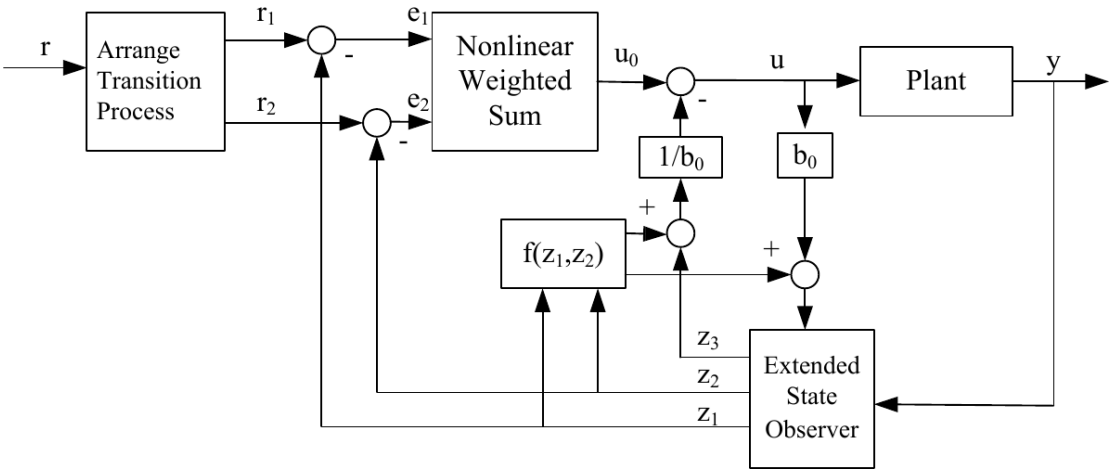

Figure 2. ADRC with model compensation system structure.

4.1 NTD design

In order to solve the defects of classic differentiators, Prof. Han [10] and his research group proposed the concept of a nonlinear tracking differentiator by using a second order steepest switch system. The nonlinear differential tracker is used in some motion control systems. The discrete form of the output equation is

$$\begin{cases} r_1(k+1) = r_1(k) + h \cdot r_2(k) \\ r_2(k+1) = r_2(k) + h \cdot \mathrm{fhan}(r_1(k) - r(k), r_2(k), \delta, h_0) \end{cases} \tag{4.1}$$

where $r(k)$ is the input signal at k time, h is the sampling period, δ is the velocity factor, h_0 is the filtering factor, and fhan$(\cdot)$ is the optimal control synthesis function.

$$\text{fhan}(x_1, x_2, r, h_0) = -\begin{cases} \delta \,\text{sign}(a), & |a| > d \\ \delta \frac{a}{d}, & |a| \leqslant d \end{cases} \tag{4.2}$$

sign$(\cdot)$ is the sign function.

$$a = \begin{cases} x_2 + \frac{a_0 - d}{2} \,\text{sign}(y), & |y| > d_0 \\ x_2 + \frac{y}{h_0}, & |y| \leqslant d_0 \end{cases} \qquad \begin{cases} d = \delta h_0 \\ d_0 = h_0 d \\ y = x_1 + h_0 x_2 \\ a_0 = \sqrt{d^2 + 8\delta\,|y|} \end{cases} . \tag{4.3}$$

The main effect of the feed forward tracking differentiator is for a given transition process with a reasonable arrangement of the input signal and extraction of the reference input signal $r_1(k)$ and differential signal $r_2(k)$ that it can reduce the influence of measurement noise on the control system performance.

4.2 ESO design

The extended state observer is a new kind of state observer that can track the all-order state variables, as well as estimate and compensate unmodeled dynamics and total external disturbance of the system. It uses nonlinearity to realize the dynamic feedback linearization of nonlinear systems. The extended state observer uses a dynamic process that only employs the input and output information of the plant instead of the transfer function of describing objects. The principle diagram of the ESO is shown in figure 3.

The system is expressed as

$$\begin{cases} \dot{x}_1 = x_2 \\ \dot{x}_2 = f(x_1, x_2) + bu \\ y = x_1 \end{cases} \tag{4.4}$$

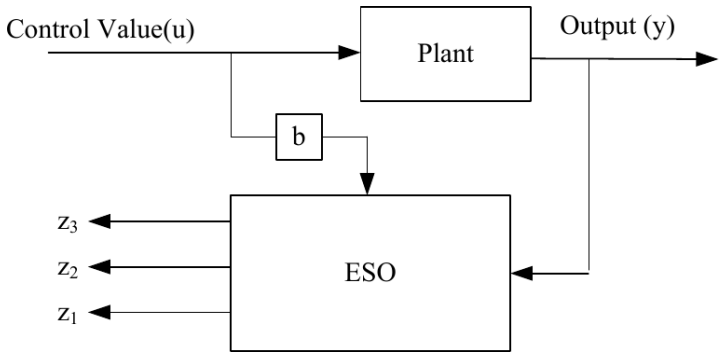

Figure 3. The principle diagram of the ESO.

where y is the output, which will be measured and controlled, u is the input, and $f(x_1, x_2)$ is a multivariable function of both the state and external disturbances. Treating $x_3(t)$ as an additional state variable, where $x_3(t) = f(x_1, x_2)$, the original plant in (4.4) is now described as

$$\begin{cases} \dot{x}_1 = x_2 \\ \dot{x}_2 = x_3 + bu\,. \\ y = x_1 \end{cases} \tag{4.5}$$

Now, we construct a state observer, denoted as the extended state observer (ESO), in the form of

$$\begin{cases} e = z_1 - y \\ \dot{z}_1 = z_2 - \beta_1 e \\ \dot{z}_2 = z_3 - \beta_2 \,\mathrm{fal}(e, \alpha_1, \delta) + f(z_1, z_2) + bu \\ \dot{z}_3 = -\beta_3 \,\mathrm{fal}(e, \alpha_2, \delta) \end{cases} \tag{4.6}$$

where $\beta_i > 0$ $(i = 1, 2, 3)$, $\alpha_1 = 0.5$, and $\alpha_2 = 0.25$. $\mathrm{fal}(e, \alpha, \delta)$ is the saturation function, whose purpose is to inhibit signal chattering and is expressed as

$$\mathrm{fal}(e, \alpha, \delta) = \begin{cases} \frac{e}{\delta^{1-\alpha}}, & |e| \leqslant \delta \\ |e|^{\alpha}\,\mathrm{sign}(e), & |e| > \delta \end{cases} \tag{4.7}$$

where $z_1(t) \to x_1(t)$, $z_2(t) \to x_2(t)$, $z_3(t) \to x_3(t) = f_1(x_1, x_2) + (b - b_0)u(t)$.

In the (4.6), $z_3(t)$ is the expansion of the state. Using the formula for a nonlinear expansion observer (4.6), we can observe the position, speed and the unknown part of the plant. In practical control engineering, the observer can achieve control without speed measurement or implement from unknown uncertainties or external disturbance compensation.

4.3 NLSEF design

PID employs a linear combination of present, accumulative, and predictive forms of tracking errors and has ignored other possibilities for combinations that are potentially much more effective. As an alternative, the following nonlinear function is proposed:

$$\begin{cases} e_1 = r_1 - z_1 \\ e_2 = r_2 - z_2 \\ u_0 = \beta_1 \,\mathrm{fal}(e_1, \alpha_1, \delta) + \beta_2 \,\mathrm{fal}(e_2, \alpha_2, \delta), \qquad 0 < \alpha_1 < 1 < \alpha_2\,. \end{cases} \tag{4.8}$$

Compared with PID, the NLSEF cancels the integral link, avoids the integral feedback. Because the integral feedback is easy to cause defects such as integral saturation, unstable turbulence, slowness, etc.

4.4 Disturbance compensation control output

When an ESO detects the real-time action of the unknown disturbance, it can calculate the disturbance compensation. The total output of the ADRC controller is

$$u = u_0 - \frac{z_3 + f(z_1, z_2)}{b_0}\,. \tag{4.9}$$

2017 JINST 12 T03006

5 Simulation and experiment

Figure 4 shows the structure of the hexapod. Each branch chain of the hexapod is composed of an AC servo motor drive system and ball screw. Considering the identical structure of all six actuators, a decentralized control strategy is adopted to realize position control of the hexapod. This means that each actuator is controlled separately by an ADRC. The mutual coupling between the six actuators can be regarded as disturbances to handle.

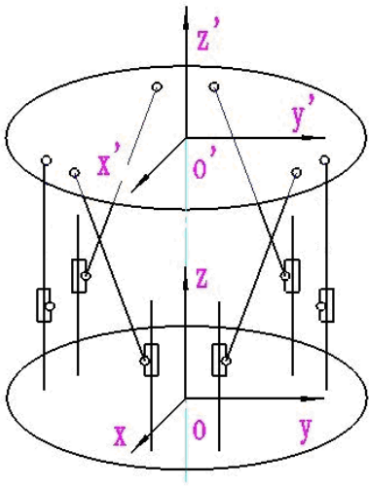

Figure 4. PSS hexapod motion model.

Figure 5 shows the control sketch of each branch chain of the hexapod. Where $J = J_{\mathrm{AC}} + J_s$ is the sum of the moment of inertia of the AC motor and the ball screw, T_e is the motor output torque, T_L is the load torque, and T_d is the unknown disturbance, including the friction. The equation $J\frac{d^2\theta}{dt^2} + B\frac{d\theta}{dt} = T_e - T_L - T_d$ describes the process of the system. Taking Laplace transform of both sides, we obtain $\frac{\theta(s)}{I(s)} = \frac{K_t}{s(Js+B)}$. When converting the angle into a linear displacement, the Laplace transform is $\frac{Y(s)}{I(s)} = \frac{K_t \times L}{2\pi s(Js+B)} = \frac{2}{s^2+32s}$. Where the torque constant is $K_t = 0.289\,\mathrm{N \cdot m/A}$, the ball screw lead is $L = 2 \times 10^{-3}\,\mathrm{m}$, the moment of inertia is $J_{\mathrm{AC}} = 0.052 \times 10^{-4}\,\mathrm{kg \cdot m^2}$, the equivalent moment of inertia of the ball screw is $J_s = 0.51456 \times 10^{-4}\,\mathrm{kg \cdot m^2}$, and the damping coefficient is $B = 1.8145 \times 10^{-3}\,\mathrm{N \cdot m/rad \cdot s^{-1}}$.

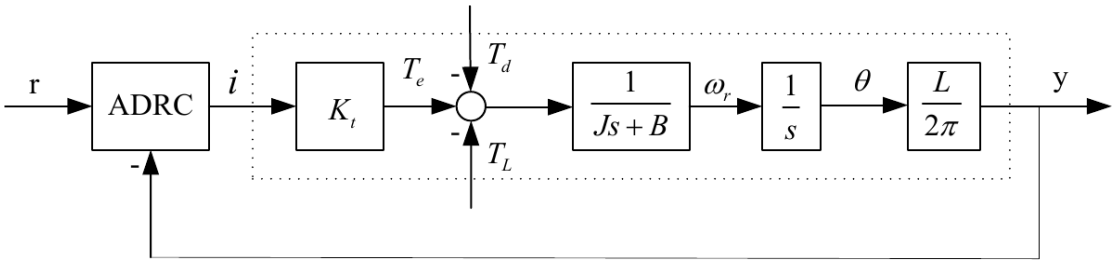

Figure 5. AC servo motor ADRC system.

To verify the effectiveness of the ADRC control method, several experiments have been conducted using the sinusoidal excitation signal, given that the hexapod is only affected by the coulomb

friction $f(z_1, z_2) = a_0 \operatorname{sign}(\dot{y})$, where $a_0 = 1$. In order to verify performance of the ADRC, the random disturbance signal is $d = 10 * \sin(t)$.

In the simulation, the system parameters are as follows:

$$h = 0.01, \quad \delta = 50$$
$$\beta_1 = 100, \quad \beta_2 = 300, \quad \beta_3 = 1000, \quad \delta_1 = 0.0025, \quad \alpha_1 = 0.5, \quad \alpha_2 = 0.25$$
$$\delta_2 = 2 * h, \quad \alpha_1 = 3/4, \quad \alpha_2 = 3/2, \quad \beta_1 = 150, \quad \beta_2 = 1\,.$$

It is evident from figure 6 that the steady-state tracking error sinusoidal excitation of the ADRC is better than the PID. From figure 7, we know that the ARDC is good for position signal, speed signal and uncertain part estimations. The simulation results indicate that the disturbance observer of the ADRC for the uncertain part has a good inhibitory effect and better robustness.

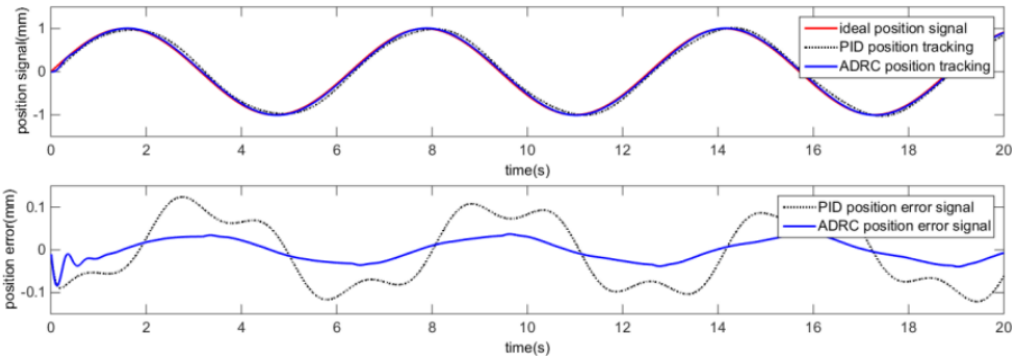

Figure 6. Position tracking error sinusoidal excitation of PID and ADRC.

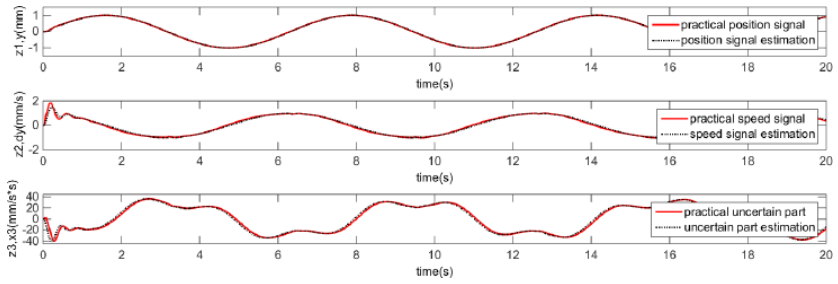

Figure 7. ESO observed result of ADRC.

We install the hexapod to the telescope and use the ADRC to design a controller. The testing apparatus is shown in figure 8 and the control system interface is shown in figure 9. Three displacement meters and an electronic autocollimation are respectively used to test the three-dimensional parallel motions and two dimensional tilts. The test results show that the absolute accuracy of the three dimensional parallel motions is about ± 4 μm, and the two dimensional tilts' is about 10 μrad. The control precision meets the system design for a telescope secondary mirror.

6 Summary

Due to the special requirements of the large aperture telescope on the secondary control system, this paper proposes a new-type of 6-DOF secondary position adjusting mechanism. We have carried

2017 JINST 12 T03006

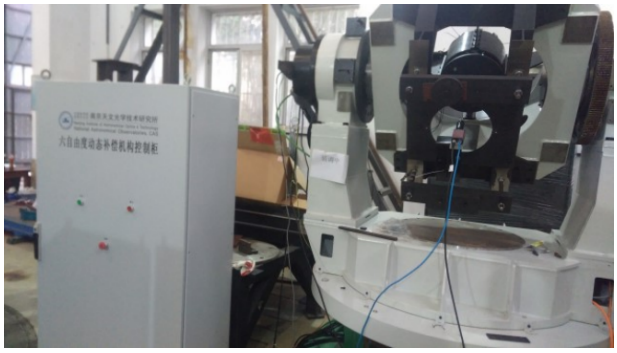

Figure 8. Testing apparatus.

Figure 9. Hexapod control system interface.

out the simulation research on the telescope hexapod parallel mechanism control problem with the ARDC control technology. The simulation results show that the ADRC control technology with model compensation can estimate and compensate for the uncertainties, compared with PID control technology, with better dynamic performance, higher tracking accuracy, and greater robustness. The test results of the absolute accuracy show that the new-type hexapod could satisfy the requirements of the telescope secondary mirror control system. It can also provide reliable technical support for establishment of larger aperture telescope in the future.

Acknowledgments

This research project is subsidized by the six degrees of freedom dynamic compensation mechanism, the Chinese Academy of Sciences, China (Grant No. 2911C09700), the study of control strategy and detection method of an improved hexapod, National Nature Science Foundation, China (Grant No. 11503060), and research on parallel control technology of the large aperture telescope's mount driving, National Nature Science Foundation, China (Grant No. 11303065).

2017 JINST 12 T03006

References

[1] P. Schipani et al., *Parallel robots in a ground-based telescope active optics system: theory and experiments*, *Proc. SPIE* **6715** (2005) 671503.

[2] R. Barho, S. Stanghellini and G. Jander, *VLT secondary mirror unit performance and test results*, *Proc. SPIE* **3352** (1998) 675.

[3] P. Schipani et al., *The VST secondary mirror support system*, *Proc. SPIE* **7018** (2008) 701845.

[4] J.M. Casalta et al., *The performances of GTC secondary mirror drive unit*, *Proc. SPIE* **5495** (2004) 507.

[5] E.H. Anderson et al., *Precision, range, bandwidth and other tradeoffs in hexapods with application to large ground based telescopes*, *Proc. SPIE* **6273** (2006) 62731F.

[6] A. Al-Homsy, J. Hartmann and E. Maehle, *Adaptive Control of Leg Position for Hexapod Robot Based on Somatosensory Feedback and Organic Computing Principles*, in proceedings of the *16th International Conference on Climbing and Walking Robots and the Support Technologies for Mobile Machines*, University of Technology, Sydney, Australia, 14–17 July 2012, K.J. Waldron, M.O. Tokhi and G.S. Virk eds., World Scientific (2013), section 4, p. 225.

[7] C.I. Huang and L.C. Fu, *Smooth sliding mode tracking control of the Stewart platform*, *IEEE Int. Conf. Control Appl.* **1** (2005) 43.

[8] G. Liang, *A kind of fault-tolerant decouple and control algorithms for non-linear and time-varying MIMO system based on neuron adaptive pid and neural network*, in proceedings of the *2007 International Conference on Wavelet Analysis and Pattern Recognition*, Beijing, China, 2–4 November 2007, volume 2, p. 677 [doi:10.1109/ICWAPR.2007.4420754].

[9] H.X. Cai et al., *Low velocity tracking control based ADRC for Large-scale Telescope System*, *Proc. SPIE* **9678** (2015) 967803.

[10] J.Q. Han, *From PID to Active Disturbance Rejection Control*, *IEEE Trans. Ind. Electron.* **56** (2009) 900.

[11] R.G. Van Silfhout, *High-precision hydraulic Stewart platform*, *Rev. Sci. Instrum.* **70** (1999) 3488.

[12] Z.Y. Yue, Y. Ye and B.Z. Gu, *Modeling and Simulation of a 6-DOF Parallel Platform for Telescope Secondary Mirror*, *Proc. SPIE* **9145** (2014) 91452P.

2017 JINST 12 T03006